Femtosecond laser microstructuring of zirconia dental implants

R. A. Delgado-Ruíz,[1] J. L. Calvo-Guirado,[1] P. Moreno,[2] J. Guardia,[3] G. Gomez-Moreno,[3] J. E. Mate-Sánchez,[1] P. Ramirez-Fernández,[1] F. Chiva[1]

[1]Faculty of Medicine and Dentistry, University of Murcia, Murica, Spain
[2]Faculty for Sciences, Laser department, University of Salamanca, Salamanca, Spain
[3]Faculty of Dentistry, University of Granada, Granada, Spain

Received 1 December 2009; revised 5 August 2010; accepted 25 August 2010
Published online 8 November 2010 in Wiley Online Library (wileyonlinelibrary.com). DOI: 10.1002/jbm.b.31743

Abstract: This study evaluated the suitability of femtosecond laser for microtexturizing cylindrical zirconia dental implants surface. Sixty-six cylindrical zirconia implants were used and divided into three groups: Control group (with no laser modification), Group A (microgropored texture), and Group B (microgrooved texture). Scanning electron microscopy observation of microgeometries revealed minimal collateral damage of the original surface surrounding the treated areas. Optical interferometric profilometry showed that ultrafast laser ablation increased surface roughness (R_a, R_q, R_z, and R_t) significantly for both textured patterns from 1.2× to 6×-fold when compared with the control group ($p < 0.005$). With regard to chemical composition, microanalysis revealed a significant decrease of the relative content of contaminants like carbon (Control 19.7% ± 0.8% > Group B 8.4% ± 0.42% > Group A 1.6% ± 0.35%) and aluminum (Control 4.3% ± 0.9% > Group B 2.3% ± 0.3% > Group A 1.16% ± 0.2%) in the laser-treated surfaces ($p < 0.005$). X-ray diffraction and Raman spectra analysis were carried out to investigate any change in the crystalline structure induced by laser processing. The original predominant tetragonal phase of zirconia was preserved, whereas the traces of monoclinic phase present in the treated surfaces were reduced (Control 4.32% > Group A 1.94% > Group B 1.72%) as the surfaces were processed with ultrashort laser pulses. We concluded that femtosecond laser microstructuring offers an interesting alternative to conventional surface treatments of zirconia implants as a result of its precision and minimal damage of the surrounding areas. © 2010 Wiley Periodicals, Inc. J Biomed Mater Res Part B: Appl Biomater 96B: 91–100, 2011.

Key Words: zirconia, dental implants, femtosecond laser, surface roughness, X-ray diffraction, Raman analysis

INTRODUCTION

Recent advances in the development of high-mechanical strength ceramics have made them attractive as new materials for dental implants. Zirconium oxide partially stabilized with yttrium (Y-TZP, yttrium-stabilized tetragonal zirconia polycrystals) offers several advantages due to its high resistance to fracture and flexural strength.[1,2] Based on histological examination, the zirconia has shown a good reaction to connective tissue and bone,[3–6] as well as excellent osseointegration observed in animal studies.[2,7–11]

To improve the biocompatibility and mechanical performance of the zirconia implants, a number of surface treatments have been recently applied. Among them, the aggregation of hydroxyapatite[12] or CaP[13] nanolayers, Mg ion implantation,[14] sandblasting with aluminum oxide particles, and simple etching with hydrochloric or hydrofluoric acids.[15,16] More recently, UV radiation was used to increase the hydrophilic properties of the zirconia surfaces.[17]

Physical and chemical microtexturizing techniques currently applied to dental implants produce various surface geometries and differing degrees of surface roughness. However, most of them are quite tricky procedures,[18] and the final result is difficult to control.[19] Additionally, they require special laboratory conditions, and they sometimes demand special conditions including contaminant-free working areas and are usually restricted to conductive materials.[20,21]

As far as zirconia is concerned, electrical techniques are precluded, and acid or alkaline-etching techniques do not give rise to high-surface roughness levels, because the original material is manufactured using high-isostatic pressure to make it resistant to chemical, physical, or wear changes[22].

The reason for these geometric, physical, or chemical modification techniques is to enhance surface-cell interactions and to stimulate cellular activity. The ultimate goal is to improve osseointegration and the bone-to-implant interface strength and resistance for long-term functional loading.[23]

Femtosecond laser microtexturing increases surface roughness, reduces the presence of residual elements, and the resulting surface retains it characteristics permanently. It is also a technique that has much potential for automation and therefore reproducibility.[24]

Laser sources have been used in the past to microstructure zirconia surfaces. In the 1990s, Minamizato[25] processed flat zirconia surfaces with pulsed Nd:YAG lasers to drill

Correspondence to: R. A. Delgado-Ruíz; e-mail: raderu78@gmail.com

500-μm diameter holes through a thickness of 2 mm at the intraosseous portion of laminar zirconia implants. He reported the presence of a layer of molten and resolidified zirconia around the holes as well as cracks all along the walls and the vicinity of the crater. A CO_2 laser was also used on laminar zirconia surfaces to enhance the polar component of the surface energy[26] and thus increase wettability and adhesion of hFOB 19 osteoblasts[27,28].

There are few studies describing the application of femtosecond laser pulses to microstructuring zirconia dental implants. Focusing on dental zirconia, microgrooves were created on the surface of Y-TZP crowns to aid dental bonding,[29] whereas dental crowns were manufactured by laser microstructuring of hot-isostatically pressed zirconia.[30]

A recent study by Stübinger et al.[31] has compared the effects of Er:YAG, CO_2, and diode lasers on the surfaces of zirconia polycristal disks. At different intensities, CO_2 and Er:YAG lasers produce undesirable effects on the surface such as microcracks, pits, and melting of the material. On the other hand, diode laser was unable to bring about any surface alteration.[31]

There are no references to microstructuring techniques with femtosecond laser on cylindrical zirconia dental implant surfaces. However, ablation with femtosecond laser pulses is a potential candidate to become a useful tool for microstructuring implant surfaces essentially because of its precision and the small thermal load on the material.

The main goal of this study was to generate high-quality microstructures (grooves and pores) on the surface of cylindrical zirconia dental implants by means of ultrafast laser ablation. At the same time, we were interested in the description and analysis of the modified surfaces to evaluate their potential to improve implant performance. Scanning electron microscopy (SEM) helped to evaluate the morphology of the surfaces. The changes in the surface roughness were quantified by means of noncontact optical interferometric profilometry. SEM elemental microanalysis allowed us to evaluate the changes in the chemical composition of the surface while phase changes after laser processing were assessed by means of X-ray diffraction and Raman spectroscopy analysis.

MATERIALS AND METHODS

Specimens by group and are illustrated in Figure 1.

Zirconia implants

Sixty-six White SKY® (Bredent medical® GMBH & Co. KG, Senden, Germany) zirconium dioxide implants of 4-mm diameter and 8-mm length were used; these were manufactured using high-pressure sintering of tetragonal zirconium oxide polycrystals stabilized with 3% molar ratio yttrium oxide at temperatures in the range of 1173–2370°C. Afterward, the implants undergo surface sandblasting with aluminum oxide particles.

The implants were divided into three groups: Control—twenty-two implants not subjected to laser treatment; Group A—twenty-two implants treated with femtosecond laser pulses to create pores 30-μm diameter, 70-μm pitch; Group B: twenty-two implants treated with femtosecond laser pulses to create grooves with 30-μm wide and 70-μm pitch (Figure 2).

Laser-microstructuring devices

A commercial Ti:Sapphire oscillator (Tsunami, Spectra Physics) and a regenerative amplifier system (Spitfire, Spectra Physics) based on chirped pulsed amplification were used for microstructuring. The system delivers 120 fs linearly polarized pulses at 795 nm with a repetition rate of 1 kHz. The transverse mode was TEM00, and the beam width was 9 mm ($1/e^2$ criterion). Pulse energy can reach a maximum of 1.1 mJ and is reduced by means of neutral filters and a half wave plate and polarizer system to generate the most suitable fluences on the surface of the material for producing ablation with minimal damage to the surrounding area.

The laser pulses travel through air to the focusing system. This consisted of an achromatic doublet lens and an off-axis imaging system (lens, beam splitters, and CCD Philips Luca® cameras that allow the visualization of the processing area, facilitating implant positioning and beam focusing. Implants were placed on a motorized platform with three-axis motion, *X*, *Y*, and *Z*, controlled by Micos ES100® software (Nanotec Electronic GMBH & Co., Munich, Germany), so that laser pulses impinge perpendicularly to the implant axis. The platform was mounted on an OWIS® rotating motorized base (Nanotec Electronic GMBH & Co.), controlled by software that turned the base at speeds varying between 0° and 30°/s, allowing the whole periphery of the implant to be texturized without altering focusing conditions (Figure 3).

The outcomes of laser were monitored and controlled using an Axio Vision® Light Microscopy reflection optical microscope (Carl Zeiss®, Göttingen Germany), with Axio Imager® M1m software (Carl Zeiss). The lenses used were high-resolution PLAN APO CS: 10×, 20×, 40×, 60×, and 100×.

Optical interferometric profilometry

A Veeko NT 1100® noncontact interferometric microscope (Wyco Systems, New York, USA) was used to quantify statistical surface roughness parameters R_a (average surface roughness), R_q (root mean square roughness), R_z (average maximum height of the surface), and R_t (maximum height of the surface).

Twenty-four zirconia implants (eight specimens by group) were examined on the analysis platform making six measurements with 20.7× magnification in VSI mode within the area 2-mm high of the intraosseous portion of the implant collar where laser processing was carried out. The sampling areas were 227.2 μm × 298.7 μm.

SEM: Surface characterization

A JEOL-6100 scanning electron microscope (SEM; Jeol, Tokyo, Japan) was used to study surface topography. The implants were degreased in ethanol solutions and desiccated with acetone. Finally, the implant surface was

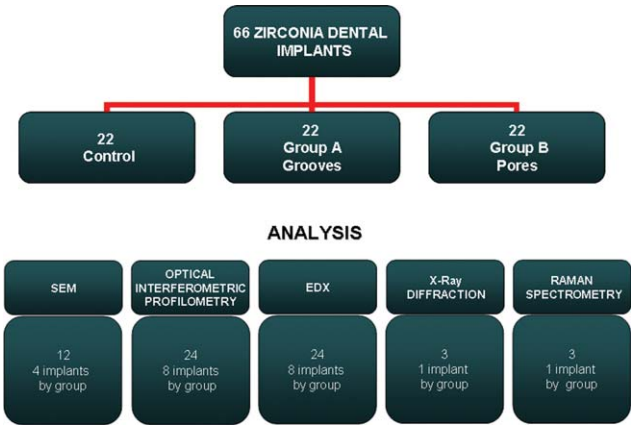

FIGURE 1. Distribution of the sample by groups and analytical techniques used. [Color figure can be viewed in the online issue, which is available at www.wileyonlinelibrary.com.]

sputtered with gold palladium in the SCD 040 (Balzers Union, Wallruf, Germany).

Twelve zirconia implants (four specimens by group) were examined. The implants were labeled and distributed radially on 4-cm diameter aluminum disks using adhesive tape, with six implants per disk.

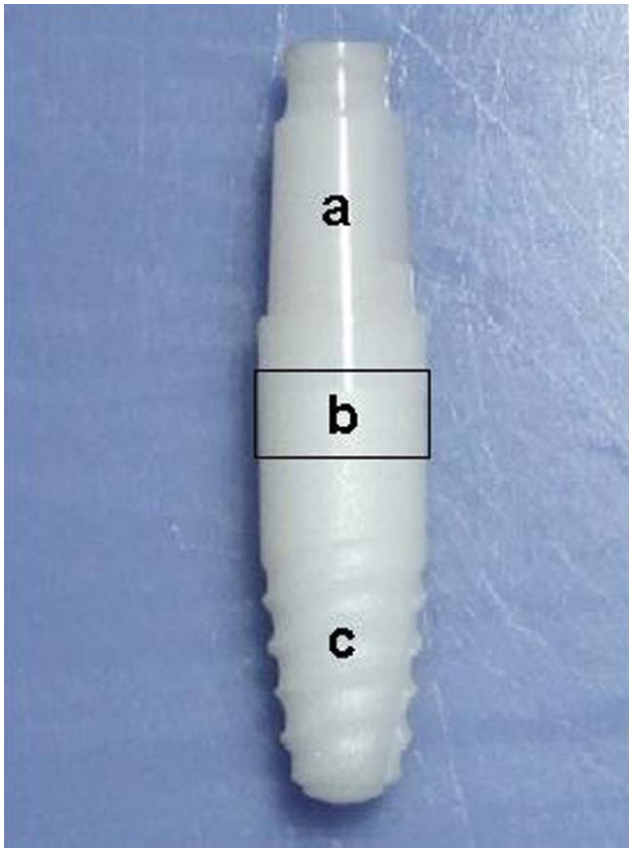

FIGURE 2. (a) Extraosseous portion of 8 mm, (b) 2-mm area that received laser processing to generate grooves or pores, and (c) intraosseous portion sandblasted by manufacturer. [Color figure can be viewed in the online issue, which is available at www.wileyonlinelibrary.com.]

Observation parameters used were a focal distance of 32 mm, 20 kV, and 450×, 1200×, 3200×, and up to 17,000× magnification.

SEM: Quantification of elements

Element analysis was carried out by energy dispersive X-ray spectroscopy using an OXFORD INCA 300 system. All the specimens were coated with a thin layer of conductive carbon in a sputter-coating unit (SCD 004 Sputter-Coater with OCD 30 attachment, Bal-Tec, Vaduz, Liechtenstein). Twenty-four zirconia implants (eight specimens by group) were analyzed. Elemental analysis was carried out in six microareas of 30 μm × 30 μm in the 2-mm area of the implant collar.

X-ray diffraction analysis

To examine the presence of the tetragonal and monoclinic ZrO_2 phases in the entire implant, three zirconia implants (one specimen by group) were embedded in epoxy resin and sectioned longitudinally using a microtome under continuous water-cooling.

The specimens were ground to a smooth surface using SiC paper with up to 1200 grit size, polished with 3-μm diamond paste and ultrasonically cleaned in a distilled water bath for 3 min. Five sections by sample were studied in an X-ray diffractometer (D8 Focus, Bruker AXS, Karlsruhe, Germany). The counting time per step was 2 s. The monoclinic phase fraction was calculated using the Garvie and Nicholson method.[32]

Raman spectrometry analysis

The cervical areas of control and laser processed implants were also analyzed by Raman spectroscopy to identify the distribution of tetragonal and monoclinic phases. We used a DeltaNu portable Raman Spectrometer, Inspector model, equipped with a NuScope microscope, an electrically refrigerated CCD camera and a diode laser at 785 nm as the excitation source (120 mW laser).

The spectra were taken in the spectral range from 200 and 2000 cm^{-1} with a resolution of 8 cm^{-1}, the final spectra resulting from the accumulation of five successive

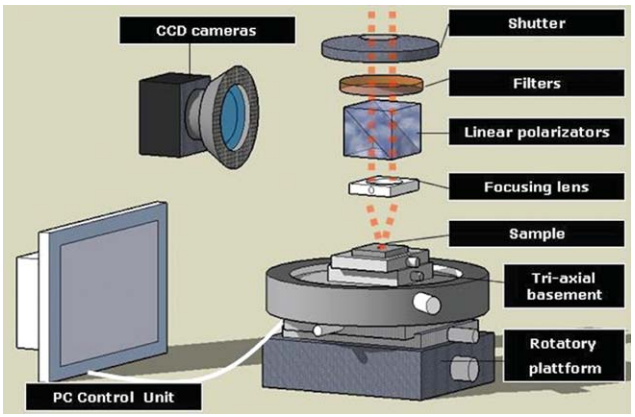

FIGURE 3. Drawing of the processing set-up. The laser beam is directed to the processing platform. [Color figure can be viewed in the online issue, which is available at www.wileyonlinelibrary.com.]

individual measurements taken from the three zirconia implants, one sample from each group.

Statistical analysis

Data obtained from optical interferometric profilometry and elemental analysis, X-ray diffraction, and Raman spectroscopy were entered into SPSS/PC version 15 software (licensed to the Murcia University).

Descriptive statistics (mean, median averages, standard deviation, and standard error) were collated for the quantitative variables R_a, R_q, R_z, and R_t, percentage in weight of chemical elements for all groups, and phase fraction was expressed in percentage.

To be sure of sample normality, the Kolmogorov–Smirnov test, the ANOVA test for independent variables, and the Bonferroni test for comparing arithmetic means between groups were applied. $p < 0.005$ was taken as significant.

RESULTS

Surface morphology

SEM images of the surface of the implants belonging to the control group showed the characteristic rough surface of the intraosseous portion edged by the polished surface of the implant transmucous section. The laser processed specimens exhibited two different surface structures. On one hand, 20 parallel lines of pores of 30-μm diameter and 70-μm pitch making a total number of 3780 pores. On the other hand, 20 helical grooves of 30-μm wide, with 70-μm pitch [Figure 4(a–c)].

Greater magnification of the control surfaces reveals crests and valleys and areas with microcracks. [Figure 5(a–c)]. Pores are circle-shaped with well-defined edges, and no further damage becomes apparent in the surface between pores. The grooves present uniform edges, and the regions between grooves show a roughened surface resembling the control surfaces. The inner surfaces of the pores exhibit granular structures ranging from some tens nanometers to some microns [Figure 5(d–f)]. Groove walls and bottom exhibited granular structures in the range of 1–2 μm and polycrystals with dimensions in the range of 5–6 μm [Figure 5(g–i)].

Further detail allows to appreciate these nanostructures that can be estimated with greater accuracy to have sizes in the range of 30–70 nm [Figure 6(a,b)].

Inside the grooves, we observe multiple polycrystal structures fixed to the walls and made up of nanometric crystal structures in the range of 50–100 nm [Figure 6(c,d)].

The grooves have a pyramidal section [Figure 7(a,b)], whereas the pores have a conical one [Figure 7(c,d)].

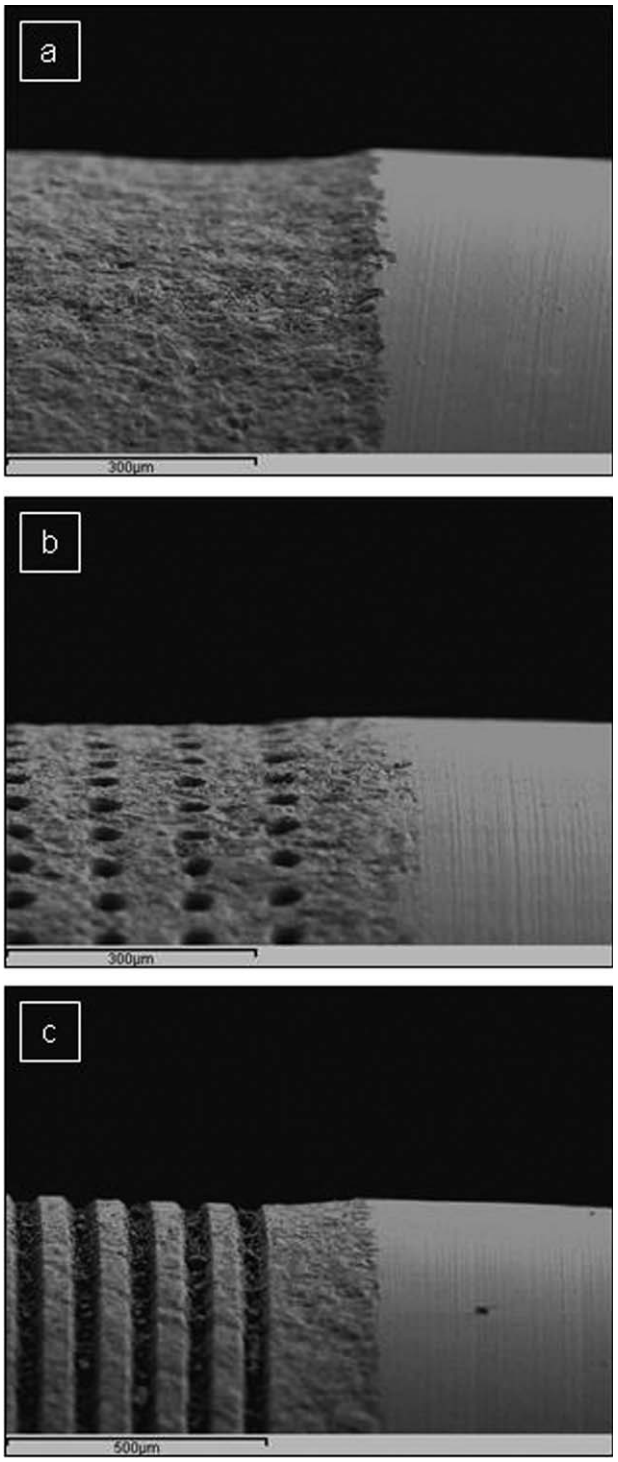

FIGURE 4. SEM images comparing surfaces. (a) Zirconia control implant, (b) zirconia pored surface, and (c) zirconia grooved surface (160× magnification).

Surface roughness

All statistical roughness parameters indicate a noticeable increase of surface roughness as a result of laser modification. The increment amounts to a factor of six for the grooved surfaces and a factor of 1.2 for pored surfaces when compared with the control group (Table I).

Elemental analysis

Table II shows the relative abundance of the main components of the zirconia together with the percentage of contaminant elements (carbon and aluminum) for the three groups of implants under investigation. The grooved and pored surfaces exhibit larger proportion of zirconium and

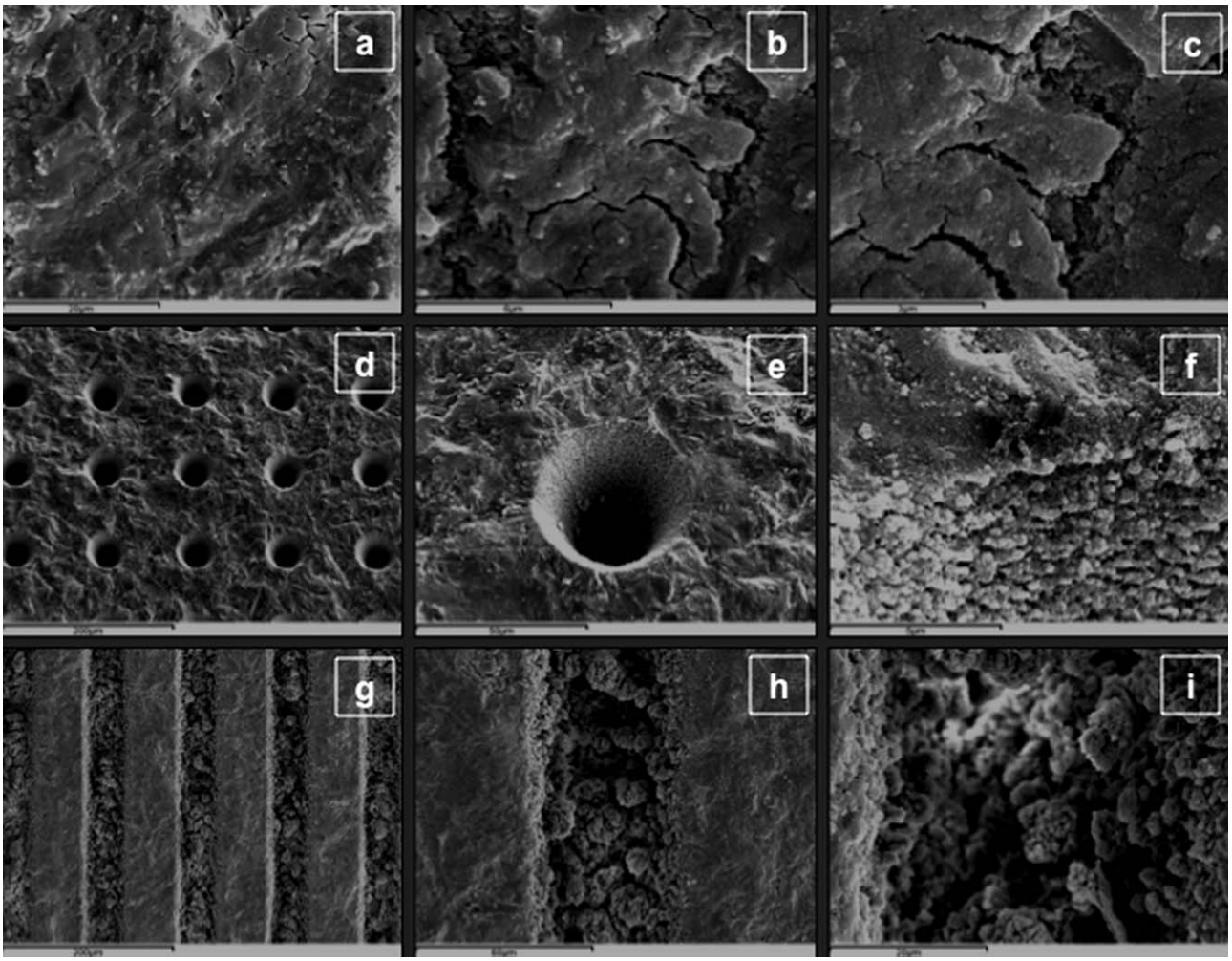

FIGURE 5. (a, b, and c) Control surface with progressive magnification; (d, e, and f) pored surface with progressive magnification, and (g, h, and i) grooved surface with progressive magnification.

oxygen than the control surfaces, whereas the presence of carbon and aluminum remarkably diminishes.

X-ray diffraction analysis

Minimal phase transformation was observed both in the control group and the laser-processed implants. The tetragonal phase was observed to be prevalent with the monoclinic phase present to a lesser extent. Monoclinic phase proportion was lower in laser-treated implants (Table III).

Raman spectroscopy analysis

Raman spectra of the implants show that the tetragonal phase is predominant both in the processed (red) and non-processed areas (blue) of the cervical collar region (Figure 8).

DISCUSSION

As it was pointed out in the introduction, as far as we know, this is the first time femtosecond laser pulses are used to generate surface patterns on zirconia dental implants. The characterization and evaluation of surface roughness, chemistry, and structure of the modified implants are mandatory.

From a biological point of view in this study, the dimensions of the microstructures were selected *a priori* to optimally guide osteoblast cellular growth. The implant collar was selected as the microstructuring target, because this is the region subjected to the strongest mechanical stress once the implant is operative.[33–39]

Microstructuring increases the effective surface of the implant and therefore helps to soften the stress in this area.[40–48] In our case, the increase was about 25% in the case of groovy pattern and 15% in the pored surface. This increase of the effective surface together with the remarkable increase of the roughness resulting from the laser ablation process (Table I) is the crucial issue that will favor mechanical retention and bone-implant interdigitation of zirconia dental implants.

Previous works reporting processing with other conventional techniques including other laser sources emphasize

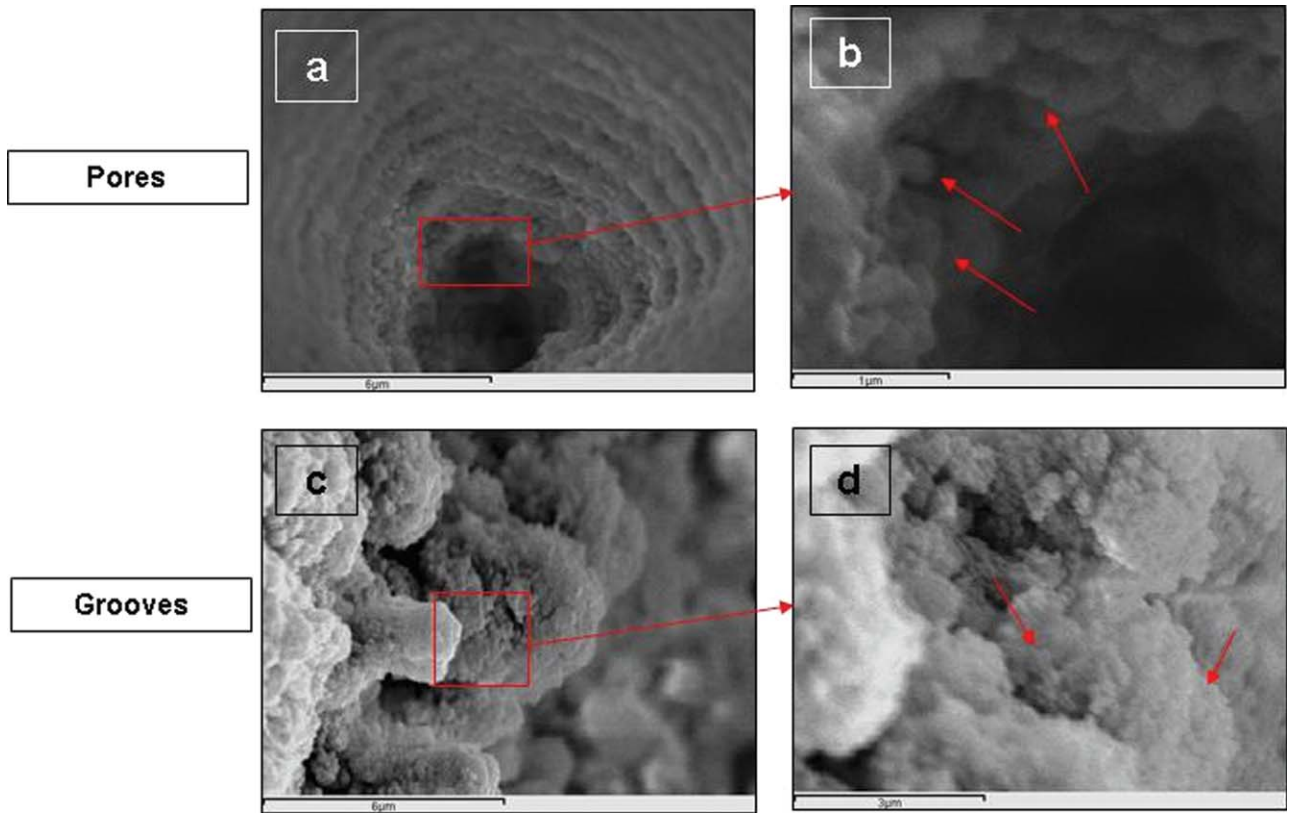

FIGURE 6. (a) Diameter of the pore decreases towards the interior giving a conical form; (b) arrows indicate the nanometer-size granules in the pore walls; (c) crystalline micrometric structures of groove wall surfaces; (d) arrows indicate the nanometer-size crystals in the pore walls. [Color figure can be viewed in the online issue, which is available at www.wileyonlinelibrary.com.]

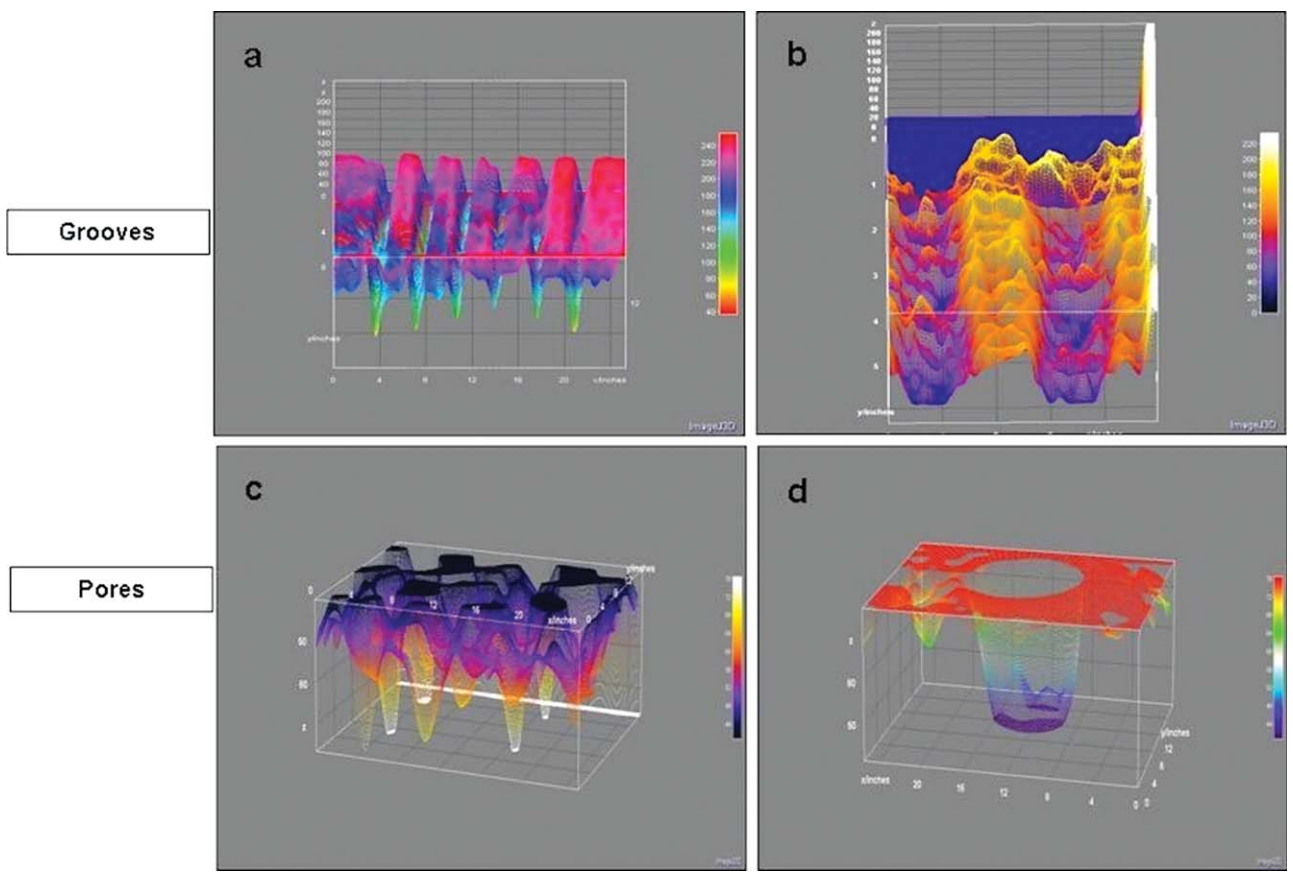

FIGURE 7. (a and b) Groove's inverted pyramid shape with truncated base; (c and d) Pore's conical shape with truncated base. [Color figure can be viewed in the online issue, which is available at www.wileyonlinelibrary.com.]

TABLE I. Surface Roughness Parameters R_a, R_q, R_z, and R_t Expressed as Micrometer (Mean Averages ± Standard Deviation)

Sample	R_a (μm)	R_q (μm)	R_z (μm)	R_t (μm)
Control ($n = 8$)	1.58 ± 0.6	2.02 ± 0.43	15.8 ± 0.5	23.63 ± 0.32
Pores (Group A) ($n = 8$)	2.43 ± 0.6*	3.48 ± 0.30*	40.42 ± 0.25*	52.68 ± 0.9*
Grooves (Group B) ($n = 8$)	9.50 ± 0.25*	11.51 ± 0.31*	55.74 ± 0.28*	60.36 ± 0.22*

* $p < 0.005$.

the collateral effects[19,22,48] that could jeopardize the aim of improving the biocompatibility and mechanical performance of the zirconia implant.

Surface treatments often leave traces of contaminants as a result of the physical or chemical processes the samples undergo. Among them, oxides, metals, metal ions, lubricants, detergents, or other specific chemical compounds. They can alter substantially the surface properties even if their amount is small, affecting the mechanical behavior of the implant or compromising its biocompatibility.[48]

In this sense, ultrafast laser microstructuring is a really clean technique as the results of elemental analysis have demonstrated (Table II). Previous mechanical processing of the implant provided the surfaces with a considerable content of aluminum and carbon. Because these impurities were just located in the periphery of the implant, ablation with femtosecond pulses removed most of them from the microstructured regions.

Because of potential heating associated with conventional lasers, it might be anticipated that crystalline phase changes would be present in the surface or bulk of the implant material. So far, one should expect this kind of effects to be present in our experiments. The predominant crystalline phase of zirconia in the implants under investigation is the tetragonal one. However, it was recently reported by Zinelis et al.[49] the presence of monoclinical phase in the same model of commercial implant that they attribute to the manufacturing process, specifically machining and grinding steps. This presence was restricted to the implant surface and was absent in the bulk. They based their conclusions on the results of X-ray diffraction and Raman spectroscopy analysis.

The analysis of X-ray diffraction and Raman spectra of the laser microstructured regions allows to extract some interesting conclusions. First, we can confirm the presence of a fraction of monoclinic phase (Table III) in the control group as it was reported in the aforementioned work of Zinelis et al.[49] More important, the fraction of monoclinic phase in the microstructured regions is much smaller than in the control group surfaces.

The explanation is twofold. On the one hand, the removal of the surface layers to create microstructures 30–50-μm deep means blowing up most of the monoclinic phase produced during manufacturing of the implants. But it also means that femtosecond laser ablation mechanism do not induce phase transformations in the material surrounding the irradiated areas.

Raman spectra of the processed and raw surfaces hold up these statements. In Figure 9, the peaks corresponding to the predominant tetragonal phase at 639, 604, 463, 314, and 268 cm^{-1}[50] are present both in the control and processed surfaces.

Unfortunately, many of the characteristic peaks of the monoclinic phase are below the lower limit of our spectral range. Nevertheless, other peaks corresponding to the monoclinic phase are located within our spectral range[49] and are absent. The only hint of the presence of monoclinic phase is the knee in the spectrum of the control surface at 755 cm^{-1}. And this peak disappeared in the spectra corresponding to the microstructured surfaces. The absence of any peak corresponding to other than tetragonal phase in the spectra of the processed areas supports both the removal of the existing monoclinic phase as well as the negligible effect of femtosecond laser ablation on the crystalline structure of the regions limiting with the microstructures.

To understand why ultrafast laser processing is so respectful with the properties of the material surrounding the microstructured regions, it is compulsory to explain the mechanism of interaction of these short pulses with matter leading to ablation.[51,52]

Briefly, ultrafast laser ablation is based on the nonlinear processes of light absorption and ionization unleashed by the effect of irradiation with very short and intense pulses. Focusing on dielectrics, within the duration of such a short pulse, a thin layer on the surface of the material is almost fully ionized. Because the electric transport properties of

TABLE II. Elements Present in Surface Chemical Composition Expressed as Percentages (Mean ± Standard deviation)

Energy dispersive X-ray spectroscopy surface analysis	C %	Al %	O %	Zr %
Control ($n = 8$)	19.7% ± 0.8%	4.3% ± 0.9%	12.6% ± 0.5%	60.2 ± 0.7%
Pores (Group A) ($n = 8$)	8.4% ± 0.42%*	2.3% ± 0.3%*	16.8% ± 0.2%*	69.3% ± 0.15%*
Grooves (Group B) ($n = 8$)	1.6% ± 0.35%*	1.16% ± 0.2%*	18.1%± 0.12%*	78.3% ± 0.2%*

* $p < 0.005$.

TABLE III. X-Ray Diffraction Analysis

Sample	Monoclinic fraction (% vol)
Zirconia control ($n = 1$)	4.32
Zirconia pores (Group A) ($n = 1$)	1.94*
Zirconia grooves (Group B) ($n = 1$)	1.72*

Monoclinic fraction expressed as percentage after five measures by implant (mean average).

* $p < 0.005$.

the material are very poor, the surface becomes charged and an ultraintense "quasielectrostatic" field between the free electrons and the ions is created. This electrostatic force may become greater than the binding force among of the ions and drag them out of the solid. This mechanism is known as Coulomb explosion and is a purely nonthermal process. Because the typical times for coupling between the electronic subsystem and the lattice are longer than some picoseconds, the material is removed before any transfer of energy to the lattice become relevant. Therefore, we should not expect any collateral effect related to heat conduction as it is usual when processing with conventional lasers (nanosecond or longer pulses).

It is worth noting that because the ionization is achieved quickly within the pulse duration, the detached electrons can still absorb energy from the laser pulse in the presence of the lattice atoms and ions by means of inverse Bremsstrahlung mechanism.[53] This absorbed energy is radiated by the plasma of electrons and contributes to raise the temperature of a deeper surface layer by electron heat diffusion to a value close to the thermodynamic critical temperature giving rise to a phase-explosion process.

This is a thermal process that becomes more relevant as the pulse energy or number increases. However, the process is still very fast and most of the energy transferred to the material is transported by the ablation products. So far, the region adjacent to the ablation zone affected by heat is restricted to a few microns, depending on the pulse energy.[54,55] The laser-processing parameters used in our work to produce the desired microstructures was not able to induce several thermal damage on the material.

CONCLUSIONS

We have reported that femtosecond laser microstructuring of zirconia implants gives rise to an increase of the roughness and the removal of contaminants incorporated in previous stages of manufacturing. These features have promise for improve the biocompatibility of the implant. Additionally, analysis of the processed surfaces by X-ray diffraction and Raman spectrometry show that the material surrounding the microstructures does not exhibit phase transformation as a result of an eventual strong thermal load.

These results and the understanding of the physical mechanisms leading to ultrafast laser ablation open a window of opportunities for this technique in the field of microstructuring dental implants. Further biological and

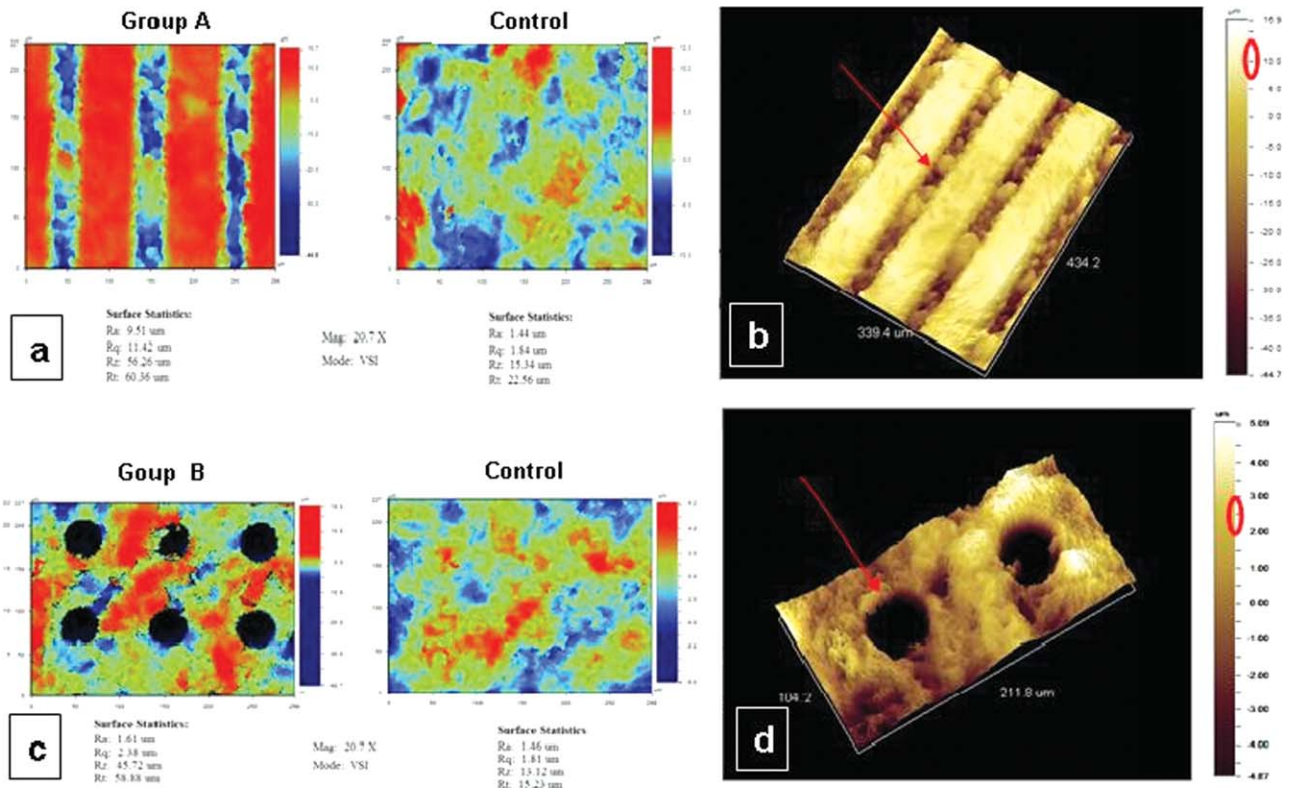

FIGURE 8. Two-dimensional and 3D comparative images of surface roughness (a). Two-dimensional image of grooves versus control group (b). Three-dimensional reconstruction of grooves (c). Two-dimensional image of pores versus control group (d). Three-dimensional reconstruction of pores. [Color figure can be viewed in the online issue, which is available at www.wileyonlinelibrary.com.]

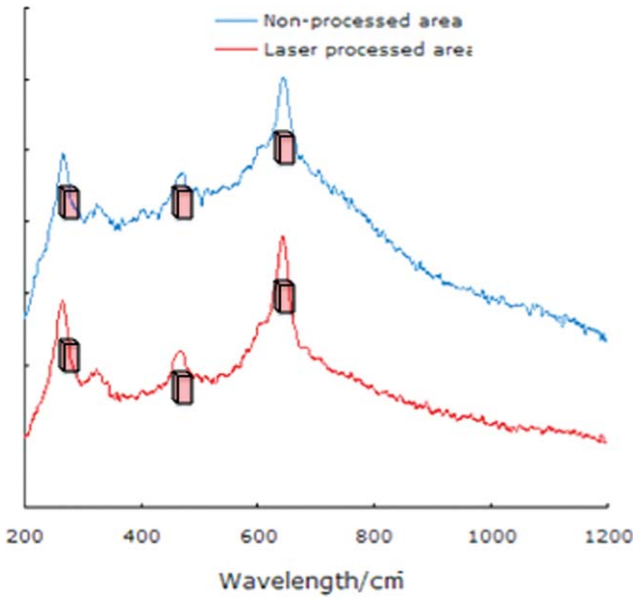

FIGURE 9. Raman spectroscopy comparison. Tetragonal peaks are label with red symbols. Monoclinic phases lower in laser processed surfaces. [Color figure can be viewed in the online issue, which is available at www.wileyonlinelibrary.com.]

mechanical tests—currently in progress—should demonstrate the degree of benefit of this technique when compared with conventional methods.

REFERENCES

1. Piconi C, Maccauro G. Zirconia as a ceramic biomaterial. Biomaterials 1999;20:1–25.
2. Albrektsson T, Sennerby L, Wennerberg A. State of the art of oral implants. Periodontol 2008;47:15–26.
3. Sennerby L, Dasmah A, Larsson B, Iverhed M. Bone tissue responses to surface-modified zirconia implants: A histomorphometric and removal torque study in the rabbit. Clin Implant Dent Relat Res 2005;7:S13–S20.
4. Christel PS. Zirconia: The second generation of ceramics for total hip replacement. Bull Hosp Jt Dis Orthop Inst 1989;49:170–177.
5. Ichikawa Y, Akagawa Y, Nikai H, Tsuru H. Tissue compatibility and stability of a new zirconia ceramic in vivo. J Prosthet Dent 1992;68:322–326.
6. Covacci V, Bruzzese N, Maccauro G, Andreassi C, Ricci GA, Piconi C, Marmo E, Burger W, Cittadini A. In vitro evaluation of the mutagenic and carcinogenic power of high purity zirconia ceramic. Biomaterials 1999;20:371–376.
7. Akagawa Y, Ichikawa Y, Nikai H, Tsuru H. Interface histology of early loaded partially stabilized zirconia endosseous implant in initial bone healing. J Prosthet Dent 1993;69:599–604.
8. Albrektsson T, Hansson HA, Ivarsson B. Interface analysis of titanium and zirconium bone implants. Biomaterials 1985;6:97–101.
9. Scarano A, Di Carlo F, Quaranta M, Piatelli A. Bone response to zirconia ceramic implants: An experimental study in rabbits. J Oral Implantol 2003;29:8–12.
10. Kohal RJ, Wolkewitz M, Hinze M, Han JS, Bächle M, Butz F. Biomechanical and histological behavior of zirconia implants. An experiment in the rat. Clin Oral Impl Res 2009;20:333–339.
11. Langhoff JD, Voelter K, Scharnweber D, Schnabelrauch M, Schlottig F, Hefti T, Kalchofner K, Nuss K, von Rechenberg B. Comparison of chemically and pharmaceutically modified titanium and zirconia implant surfaces in dentistry: A study in sheep. Int J Oral Maxillofac Surg 2008;37:1125–1132.
12. Rocchietta I, Fontana F, Addis A, Schupbach P, Simion M. Surface-modified zirconia implants: Tissue response in rabbits. Clin Oral Impl Res 2009;20:844–850.
13. Lee J, Sieweke JH, Rodriguez NA, Schüpbach P, Lindström H, Susin C, Wikesjö UM. Evaluation of nano-technology-modified zirconia oral implants: A study in rabbits. J Clin Periodontol 2009; 36:610–617.
14. Liang H, Wan YZ, Hea F, Huang Y, Xu JD, Li JM, Wang YL, Zhao ZG. Bioactivity of Mg-ion-implanted zirconia and titanium. Appl Surf Sci. 2007;253:3326–3333.
15. Gahlert M, Gudehus T, Eichhorn S, Steinhauser E, Kniha H, Erhardt W. Biomechanical and histomorphometric comparison between zirconia implants with varying surface textures and a titanium implant in the maxilla of miniature pigs. Clin Oral Impl Res 2007;18:662–668.
16. Gahlert M, Röhling S, Sprecher CM, Eichhorn S, Steinhäuser E, Wieland M, Kniha H, Milz S. Osseointegration of zirconia dental implants with a new rough surface. A biomechanical and histological study in mini pig. Eur Cell Mater 2008;16:34.
17. Att W, Takeuchi M, Suzuki T, Kubo K, Anpo M, Ogawa T. Enhanced osteoblast function on ultraviolet light-treated zirconia. Biomaterials 2009;30:1273–1280.
18. Martin JY, Schwartz Z, Hummert TW, Schraub DM, Simpson J, Lankford J Jr, Dean DD, Cochran DL, Boyan BD. Effect of titanium surface roughness on proliferation, differentiation, and protein synthesis of human osteoblast like cells (MG63). J Biomed Mater Res 1995;29:389–401.
19. Gaggl A, Schultes G, Müller WD, Kärcher H. Scanning electron microscopical analysis of laser-treated titanium implant surfaces a comparative study. Biomaterials 2000;21:1067–1073.
20. ter Brugge PJ, Wolke JG, Jansen JA. Effect of calcium phosphate coating crystallinity and implant surface roughness on differentiation of rat bone marrow cells. J Biomed Mater Res 2002;60:70–78.
21. Rajnicek AM, Britland S, McCaig CD. Contact guidance of CNS neurites on grooved quartz: Influence of groove dimensions, neuronal age and cell type. J Cell Sci 1997;110:2905–2913.
22. Kurella A, Dahotre NB. Review paper: Surface modification for bioimplants: The role of laser surface engineering. J Biomater Appl 2005;20:5–50.
23. Ellingsen JE, Thomsen P, Lyngstadaas S. Advances in dental implant materials and tissue regeneration. Periodontology 2006;41:136–156.
24. Baüerle D. Laser processing and chemistry: Recent developments. Appl Surf Sci 2002;186:1–6.
25. Minamizato T. Slip-cast zirconia dental roots tunnels drilled by laser process. J Prosthet Dent 1990;63:677–684.
26. Hao L, Lawrence J, Chian KS. Effects of CO_2 irradiation on the surface properties of magnesia-partially stabilised zirconia (MgO-PSZ) bioceramic and the subsequent improvements in human osteoblast cell adhesion. J Biomater Appl 2004:19:81–105.
27. Hao L, Lawrence J, Chian KS. Osteoblast cell adhesion on a laser modified zirconia based bioceramic. J Mater Sci Mater Med 2005; 16:719–726.
28. Hao L, Lawrence J. Effects of Nd:YAG laser treatment on the wettability characteristics of a zirconia-based bioceramic. Opt Lasers Eng 2006;44:803–814.
29. Bärsch N, Barcicowski S, Baier K. Ultrafast laser processed zirconia and its adhesion to dental cement. J Laser Micro Nano Eng 2008;3:78–83.
30. Bärsch N, Werelius K, Barcikowski S, Liebana, F.; Stute, U. & Ostendorf. Femtosecond laser microstructuring of hot-isostatically pressed zirconia ceramic. J Laser Appl 2007;19:107–115.
31. Stübinger S, Homann F, Etter C, Miskiewicz M, Wieland M, Sader R. Effect of Er:YAG. CO_2 and diode laser irradiation on surface properties of zirconia endosseous dental implants. Lasers Surg Med 2008;40:223–228.
32. Garvie RC, Nicholson PS. Phase analysis in zirconia systems. J Am Ceram Soc 2006;55:303–305.
33. Adell R, Lekholm U, Rockler B, Brånemark PI. A 15-year study of osseointegrated implants in the treatment of the edentulous jaw. Int J Oral Surg 1981;10:387–416.
34. Albrektsson T, Zarb G, Worthington P, Eriksson AR. The long-term efficacy of currently used dental implants: A review and proposed criteria of success. Int J Oral Maxillofac Implants 1986;1: 11–25.

35. Adell R, Lekholm U, Rockler B, Brånemark PI, Lindhe J, Eriksson B, Sbordone L. Marginal tissue reactions at osseointegrated titanium fixtures (I). A 3-year longitudinal prospective study. Int J Oral Maxillofac Surg 1986;15:39–52.
36. Lindquist LW, Rockler B, Carlsson GE. Bone resorption around fixtures in edentulous patients treated with mandibular fixed tissue-integrated prostheses. J Prosthet Dent 1988;59:59–63.
37. Berglundh T, Persson L, Klinge B. A systematic review of the incidence of biological and technical complications in implant dentistry reported in prospective longitudinal studies of at least 5 years. J Clin Periodontol 2002;29:197–212.
38. Engquist B, Åstrand P, Dahlgren S, Engquist E, Feldmann H, Gröndahl K. Marginal bone reaction to oral implants: A prospective comparative study of Astra Tech and Branemark System implants. Clin Oral Implants Res 2002;13:30–37.
39. Åstrand P, Engquist B, Dahlgren S, Gröndahl K, Engquist E, Feldmann H. Astra Tech and Branemark system implants: A 5-year prospective study of marginal bone reactions. Clin Oral Implants Res 2004;15:413–420.
40. Calvo-Guirado JL, Ortiz-Ruiz AJ, López-Marí L, Delgado-Ruiz R, Maté-Sánchez J, Bravo Gonzalez LA. Immediate maxillary restoration of single-tooth implants using platform switching for crestal bone preservation: A 12-month study. Int J Oral Maxillofac Implants 2009;24:275–281.
41. Abrahamsson I, Berglundh T. Tissue characteristics at micro threaded implants: An experimental study in dog. Clin Implant Dent Relat Res 2006;8:107–113.
42. Nevins M, Nevins ML, Camelo M, Boyesen JL, Kim DM. Human histologic evidence of a connective tissue attachment to a dental implant. Int J Periodontics Restorative Dent 2008;28:111–121.
43. Weiner S, Simon J, Ehremberg DS, Zweig B, Ricci JL. The effects of laser microtextured collars upon crestal bone levels of dental implants. Implant Dent 2008;17:217–228.
44. Alexander H, Ricci JL, Hrico GJ. Mechanical basis for bone retention around dental implants. J Biomed Mater Res B Appl Biomater 2009;88:306–311.
45. Geng JP, Ma QS, Xu W, Tan KB, Liu GR. Finite element analysis of four thread form configurations in a stepped screw implant. J Oral Rehab 2004;31:233–239.
46. Bratu EA, Tandlich M, Shapira L. A rough surface implant neck with microthreads reduces the amount of marginal bone loss: A prospective clinical study. Clin Oral Impl Res 2009;20: 827–832.
47. Baggi L, Capelloni I, Maceri F, Vairo G. Stress based performance evaluation of osseointegrated dental implants by finite element simulation. Simul Modell Practice Theory 2008;16:971–987.
48. Massaro C, Rotolo P, De Ricardis F, Milella E, Napoli A, Wieland M, Textor M, Spencer ND, Brunette DM. Comparative investigation of the surface properties of commercial titanium dental implants, Part 1: Chemical composition. J Mater Sci: Mater Med 2002;13:535–548.
49. Zinelis S, Thomas A, Syres K, Silikas N, Eliades G. Surface characterization of zirconia dental implants. Dent Mater 2010;26: 295–305.
50. Fernandez-Lopez E, Sánchez-Escribano M, Panizza M, Carnasciali M, Busca G. Vibrational and electronic spectroscopic properties of zirconia powders. J Mater Chem 2001;11:1891–1897.
51. Hertel IV, Stoian R, Ashkenasi D, Rosenfeld A, Campbell EB. On the physics of material processing with femtosecond lasers. RIKEN Rev 2001;32:23.
52. Jeschke HO, Garcia ME, Bennermann KH. Theory for the ultrafast ablation of graphite films. Phys Rev Lett 2001;87:1–14.
53. Meeker J, Segall AE, Semak W. Surface effects of alumina ceramics machined with femtosecond lasers. J Laser Appl 2010; 22:7–12.
54. Perrie M, Rushton A, Fox P, O'Neill W. Femtosecond laser microstructuring of alumina ceramics. Appl Surf Sci 2005;248: 213–217.
55. Sung HK, Suhn IB, Jeong S. Ablation characteristics of aluminium oxide and nitride ceramics during femtosecond laser micromachining. Appl Surf Sci 2009;255:9717–9720.